

Stress- and frequency-dependent properties of relaxor-like sodium bismuth titanateKevin Riess ¹, Neamul H. Khansur ^{1,*}, Alexander Martin^{1,2}, Andreja Benčan ³, Hana Uršič ³, and Kyle G. Webber¹¹Department of Materials Science and Engineering, Friedrich-Alexander-Universität Erlangen-Nürnberg (FAU), 91058 Erlangen, Germany²Department of Life Science and Applied Chemistry, Graduate School of Engineering, Nagoya Institute of Technology,

Nagoya 466–8555, Japan

³Electronic Ceramics Department, Jožef Stefan Institute, Ljubljana 1000, Slovenia

(Received 23 November 2020; revised 27 January 2021; accepted 8 March 2021; published 26 March 2021)

Despite the importance of $(\text{Na}_{1/2}\text{Bi}_{1/2})\text{TiO}_3$ as an end member in lead-free ferroelectrics and as an oxide ion conductor, the relaxor/ferroelectric nature remains unclear. In order to understand the relaxor-like behavior, frequency-dependent macroscopic mechanical measurements of polycrystalline $(\text{Na}_{1/2}\text{Bi}_{1/2})\text{TiO}_3$ were performed as a function of poling state, revealing the role of a potential field-induced long-range ferroelectric order on the nonlinear hysteretic stress-strain behavior. The mechanical measurements showed an increase in remanent strain and decrease in coercive stress with electrical poling, consistent with previous studies of relaxors. Electrical poling and mechanical texturing were found to influence the frequency dispersion of the relative permittivity, highlighting the potentially relaxor-like response. Further, the relative permittivity showed a directional dependence with respect to the previously applied electrical and mechanical fields. These data are discussed in conjunction with *ex situ* stress- and electric-field-dependent piezoresponse force microscopy measurements that revealed a clear ferroelectric domain switching through the application of a sufficiently high electric field, but no change of the domain configuration for uniaxial compressive stresses up to -750 MPa. The *in situ* stress-dependent crystal structure, which was characterized using synchrotron x-ray diffraction, however, indicates stress-induced ferroelastic domain switching as the primary hysteretic process.

DOI: [10.1103/PhysRevB.103.094113](https://doi.org/10.1103/PhysRevB.103.094113)**I. INTRODUCTION**

Due to the toxicity of lead and the resulting restrictions, there have been extensive studies to develop lead-free piezoelectric materials. Among others, sodium bismuth titanate $[(\text{Na}_{1/2}\text{Bi}_{1/2})\text{TiO}_3]$, NBT and its solid solutions are considered as promising candidates to replace the widely used lead zirconate titanate $[\text{Pb}(\text{Zr}, \text{Ti})\text{O}_3]$, PZT in electromechanical transducer applications, such as actuators and sensors as well as energy systems [1]. Recently, there has been considerable interest in the development of high energy density solid state energy storage systems, where NBT-based materials have also received significant interest for the exceptional large-field electromechanical response [2]. In addition, in 2013, Li *et al.* [3] reported excellent oxygen-ion conducting properties through minor concentrations of aliovalent dopants as well as by Bi-nonstoichiometry. This work highlighted the potential new applications of NBT in, e.g., solid-oxide fuel cells (SOFCs) and oxygen separation membranes. The significant variations of diffusivity by tailoring Bi-stoichiometry has also been used to enhance the electromechanical response of NBT-based solid solutions through the formation of core-shell microstructures [4].

Despite being discovered by Smolenskii *et al.* [5] in 1961, the crystal structure of NBT remains debated. Various investigations have suggested a number of possible crystal phases

at ambient temperature, including rhombohedral ($R3c$) [6–8], monoclinic (Cc) [9–11], a mixture of these structures [12], and tetragonal ($P4bm$) platelets embedded in a rhombohedral matrix [13–15]. Such discrepancies may be related to the difference between the local and the average structure (≥ 10 Å), which leads to varying results depending on the measurement technique [11]. Moreover, the origins of the large-field electromechanical behavior of NBT remains unclear. At the time of its discovery, NBT was considered to be ferroelectric [5], but the appearance of a double hysteresis loop at elevated temperatures was suggested to be antiferroelectric in nature [16]. Additionally, the temperature-dependent dielectric response shows relaxor-like characteristics, although, these are not as significant as in classical relaxors, like $\text{Pb}(\text{Mg}_{1/3}\text{Nb}_{2/3})\text{O}_3$ [17,18]. The result is an ambivalent description of the material either as a ferroelectric [5,16,19,20] or as a relaxor [21–26].

To date, however, there has not been a systematic investigation of the ferroelastic response of NBT. Such information is crucial for applications, as high stresses may arise due to, e.g., strain incompatibility and/or thermal expansion mismatch of different components [27,28]. In multilayer structures such as SOFCs (anode/electrolyte/cathode) or capacitors (ceramic/metal/ceramic), high stresses are induced due to the varying degree of thermal expansion of different components during heating and cooling cycles. This can result in material failure. Therefore, a detailed understanding of the mechanical response is required to evaluate the material performance [28]. Furthermore, the frequencies can vary considerably in operation, which makes it important to understand the

*Corresponding author: neamul.khansur@fau.de

frequency-dependent mechanical behavior, in particular because relaxors show a strong frequency dispersion [27,29]. More recently, mechanical measurements have also been successfully used to investigate the field-induced formation of long-range ferroelectric order in relaxors, as they do not suffer from conductivity issues [27,30].

According to Cross [31], typical relaxors exhibit three characteristic features: (I) the relative permittivity has a broad frequency-dependent maximum, which is not related to a crystallographic phase change, (II) a nonlinear response with limited hysteresis occurs in high alternating electric fields, and (III) no macrovolume change to a polar phase arises. Interestingly, NBT does not fulfill all three characteristics. A broad permittivity maximum without a structural transformation in combination with a frequency-dependent anomaly is apparent [32]. However, there is no frequency-dependent shift of the permittivity maximum [33]. In addition, an applied electric field results in a polarization-electric field-loop (P-E loop) characteristic of ferroelectric materials until approximately 160 °C [34,35]. Above this temperature, both antiferroelectric as well as relaxor characteristics, were detected [16,36]. The absence of a transition to a polar phase related to the formation of polar nanoregions (PNRs) [37], which is typical for relaxors [32], has been shown. In contrast to this observation, however, lamellar or irregularly shaped domains were also observed, [38,39] which may contain nanoscaled domains that exhibit PNR-like characteristics [37].

The dynamics of PNRs are related to their temperature-dependent size, below a critical temperature the thermal fluctuations slow down and the material may undergo a transition from the ergodic to the nonergodic state [40]. Considering nonergodic relaxors, the material can transform into a ferroelectric state by applying a sufficiently high electric field, which makes it difficult to differentiate them from a normal ferroelectric material in the poled state [40]. However, upon heating, the electric-field-induced ferroelectric order is broken by increased thermal energy, and the material reverts back into the ergodic state, resulting in a characteristic sharp increase in permittivity, often referred to as the ferroelectric-to-relaxor transition temperature (T_{F-R}). The field-induced ferroelectric state in relaxors can also be achieved by applied mechanical stress, which was shown for $(\text{Na}_{1/2}\text{Bi}_{1/2})\text{TiO}_3\text{-BaTiO}_3$ (NBT-BT) compositions near the morphotropic phase boundary (MPB) [41]. The dielectric anomaly (T_{F-R}) observed in the permittivity-temperature curves of the electrically or mechanically induced ferroelectric phase can be used to identify relaxor behavior. However, the existence of a T_{F-R} in NBT has not been clarified yet [42,43]. Additionally, Martin *et al.* [27] showed a significant change in the frequency-dependent behavior of the electromechanical response for relaxor NBT-BT in the unpoled and electrical poled state, which was due to a different frequency responses of the relaxor state and the field-induced ferroelectric order. Until now, such frequency dependence has not been reported for NBT, which could provide important information on the relaxor-like nature.

In addition to the ambiguous descriptions of the relaxor state in NBT [22,25,36,44–46] there is a lack of information about its frequency-dependent mechanical properties [27,29]. Combining these experiments with the field-dependent response and structural measurement techniques can give novel

insight into the electromechanical behavior. Therefore, in this work, the macroscopic mechanical response of NBT has been investigated over a wide frequency range from 0.01 to 500 mHz and is discussed in conjunction with the temperature-dependent dielectric and piezoelectric behavior. Furthermore, to distinguish between the ferroelectric and relaxor state in NBT the *ex situ* field-dependent domain structure using piezoresponse force microscopy (PFM) and the *in situ* stress-dependent crystal structure by means of synchrotron x-ray diffraction were investigated.

II. EXPERIMENTAL METHODS

Polycrystalline $(\text{Na}_{1/2}\text{Bi}_{1/2})\text{TiO}_3$ samples were prepared with the conventional solid-state synthesis route with a bismuth-excess of 0.1 mol% to compensate for the evaporation of Bi during sintering. The high-purity raw powders: Na_2CO_3 (99.50%, Alfa Aesar), Bi_2O_3 (99.99%, Projector), and TiO_3 (99.60%, Alfa Aesar) were dried at 120 °C. To reduce the absorption of humidity, the raw materials were weighed in a glovebox with a relative humidity $\leq 10\%$. Ethanol and zirconia milling balls were added to the powders. Subsequently, the raw powders were mixed/ground for 24 h and dried, followed by two-step calcination to ensure the complete reaction of the raw materials with a dwell time of 2 and 3 h at 700 °C and 800 °C, respectively. The powder was then again mixed and ground for 24 h. After drying and sieving, the powder was cold isostatic pressed at 180 MPa. Sintering was carried out at 1150 °C for 2 h with a heating and cooling rate of 5 K/min. Finally, the samples were ground and lathed to ensure the required sample geometry for the respective measurement/analysis technique (specified in the corresponding sections). In the case of electrical measurements, the samples were electroded with Pt by sputter coating. To eliminate residual stresses, the samples were annealed before each measurement at 600 °C for 2 h with a heating and cooling rate of 5 and 1 K/min, respectively.

Elemental analysis of the sintered sample was performed using inductively coupled plasma-optical emission spectroscopy (Spectro Genesis, SPECTRO Analytical Instruments). The Na/Bi ratio was found to be 1.004 within the sensitivity of the measurement technique used here. As such, the nominal composition is considered as $\text{Na}_{1/2}\text{Bi}_{1/2}\text{TiO}_3$. The bulk density of the sintered sample was measured to be $5.90 \pm 0.01 \text{ g/cm}^3$, which refers to a relative density of 98.49% and in good agreement with previous reports [3].

Temperature-dependent measurements of the dielectric permittivity were conducted in a modified furnace (LE4/11/3216, Nabertherm) and measured with an LCR meter (E4980AL, Keysight) at frequencies between 1 and 1000 kHz, where cuboid samples ($3.00 \times 3.00 \times 4.00 \text{ mm}^3$) were heated to 400 °C with a rate of 2 K/min.

For the determination of the ferroelectric properties, a piezoelectric evaluation system (TF2000, aixACCT) connected to a high-voltage power amplifier (20/20C, Trek) was used. During the measurement, a triangular bipolar electrical field of 8 kV/mm was applied to the cylindrical samples (height: 1.0 mm, diameter: 7.1 mm) with a frequency of 100 mHz. Electrical poling was conducted with cuboid samples ($3.0 \times 3.0 \times 4.0 \text{ mm}^3$). The samples were

submerged in an oil bath and electrically poled at 80 °C with an applied electric field of 4 kV/mm for 5 min, followed by field cooling to room temperature. Subsequent characterization of electrically poled samples was performed after a minimum wait time of 24 h.

Rate-dependent ferroelastic measurements were conducted with a screw-type load frame (Z030, Zwick GmbH & Co.KG) in a frequency range from 0.01 to 500 mHz. The applied load was controlled by a load cell and the displacement was measured with a custom-built linear variable differential transformer system [47]. Cylindrical samples with a height of 6.0 mm and a diameter of 5.8 mm were loaded from an initial preload of -3.8 MPa to a maximum load of -500 MPa and unloaded with the same rate to preload. Loading rates between 0.01 MPa/s to 500 MPa/s were used. To reproduce the stress-strain response during the synchrotron x-ray measurements and for mechanical texturing of PFM samples, additional measurements were performed on cuboid samples ($3.0 \times 3.0 \times 4.0$ mm³) with a loading and unloading rate of ± 1.5 MPa/s to a maximum load of -750 MPa. Before characterization of mechanically textured samples, a minimum waiting time of 24 h was used.

The temperature-dependent direct piezoelectric coefficient d_{33} was measured in a temperature range from room temperature to 400 °C with a modified screw-type load frame (5967, Instron GmbH) equipped with a thermal chamber. A sinusoidal amplitude of ± 0.5 MPa was applied (frequencies: 5–110 Hz) on the sample by using a piezoelectric stack actuator (P-025.80, PI Ceramic GmbH) and the resultant polarization signal was recorded by a Sawyer-Tower circuit. The polarization and load amplitude were used to calculate the small-signal direct piezoelectric coefficient. Details of the measurement setup can be found elsewhere [48,49].

The samples for scanning transmission electron microscopy (TEM) and selected area electron diffraction (SAED) analysis were prepared using standard TEM methods; the samples were polished down to 100 μ m and, after dimpling, finally thinned down to electron transparency using Gatan PIPS ion-milling system. TEM studies were carried out using a probe Cs-corrected Jeol ARM 200 CF STEM operated at 200 kV.

An atomic force microscope (MFP3D, Asylum Research) equipped with a PFM module, was used to determine the domain structure in dual AC resonance-tracking mode. During the measurement, an AC signal with an amplitude of 8 V and a frequency of 350 Hz was applied. Due to the increasing piezoelectric activity of the electrically poled sample, the amplitude of the scanning AC voltage in this case was only 4 V.

In situ stress-dependent synchrotron x-ray diffraction was performed at the beamline ID31 of the European Synchrotron and Radiation Facility in Grenoble. A monochromatic x-ray beam with an energy of 37 keV and a beam size of approximately 200×200 μ m² was used. The large area 2D detector (Pilatus3 X CdTe 2 M, Dectris) collects data in a full 360° azimuth angle. Cuboid samples ($1 \times 1 \times 2$ mm³) were mounted in a custom-built compact load frame and a load of -750 MPa was applied with a loading and unloading rate of approximately ± 1.5 MPa/s. Further description of the experimental setup can be found in our previous work [41].

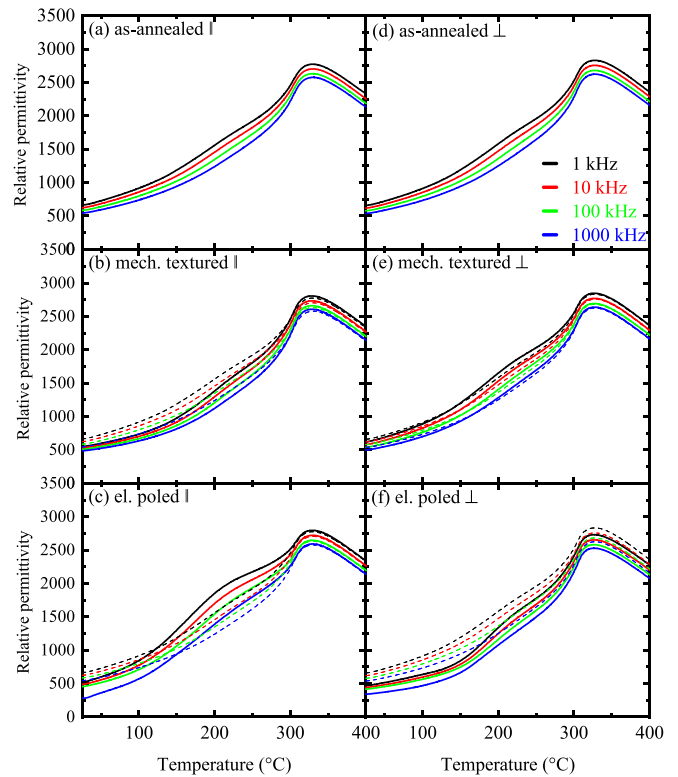


FIG. 1. Temperature-dependent relative permittivity of as-annealed, mechanically textured and electrically poled NBT measured in parallel (a), (b), (c) and perpendicular (d), (e), (f) direction to the applied fields, respectively. Experiments were performed with field-cooling-zero-field-heating. Dashed lines in (b), (c), (e), and (f) represented the data of the as-annealed sample.

Selected area peak fitting was carried out with the software package IGOR PRO.

III. RESULTS AND DISCUSSION

A. Dielectric and piezoelectric response

Figures 1(a)–1(f) shows the temperature-dependent relative permittivity of polycrystalline NBT with different poling histories at various frequencies from 25 °C to 400 °C measured parallel and perpendicular to the applied electrical and mechanical field direction. The as-annealed samples [Figs. 1(a) and 1(d)] exhibit, in addition to a frequency dependence at low temperatures, two dielectric anomalies with increasing temperature. At ~ 200 °C, a broad shoulder with an intensified frequency dependence can be seen. It is followed by a decrease in the frequency dispersion, which finally merges into a broad maximum at ~ 323 °C (T_m). Above T_m the permittivity decreases continuously. These observations are consistent with previous reports [25,35,42,50]. T_m does not shift with the measurement frequency, where a frequency-dependent permittivity maximum without a structural transformation is usually associated with relaxors. According to Jones *et al.* [8], NBT exhibits a rhombohedral ($R3c$) crystal structure up to ~ 255 °C followed by a region of coexisting rhombohedral and tetragonal ($P4bm$) structure to ~ 400 °C. Above this temperature, the tetragonal phase

is stable up to 500 °C. The rhombohedral structure in NBT is described as ferroelectric to the depolarization temperature (T_d) of ~ 200 °C [42,51,52]. In the higher temperature range until ~ 340 °C, the material response is explained either by antiferroelectric behavior [16,50] or by the formation of PNRs [22,23,51,52]. However, this does not explain the occurrence of a frequency dependence at room temperature. A possible reason is that the material exists in a nonergodic state. As such, temperature-dependent permittivity measurements of electrically poled and mechanically textured sample can highlight the existence of nonergodicity [41]. Both the electrically poled [Figs. 1(c) and 1(f)] and the mechanically textured samples [Figs. 1(b) and 1(e)] exhibit a decreased relative permittivity compared to the as-annealed sample and with the exception of the mechanically textured sample measured in perpendicular direction a reduction in frequency dispersion at low temperatures. Despite this, however, the formation of a clear T_{F-R} , marked by a dielectric anomaly at a critical temperature separating the nonergodic and ergodic relaxor states, is not developed in NBT, in contrast to other relaxor materials, such as $\text{Pb}(\text{Mg}_{1/3}\text{Nb}_{2/3})\text{O}_3$, [18] $(\text{Pb}_{1-x}\text{La}_x)(\text{Zr}_y\text{Ti}_{1-y})_{1-x/4}\text{O}_3$, [53] and NBT-BT near the MPB [21]. Please note, dielectric loss data did not show any clear anomaly that can be identified as the T_{F-R} (Fig. SI) [54]. This anomaly is understood to be due to increased thermal fluctuations resulting in the loss of long-range ferroelectric order obtained in the nonergodic state through application of electrical and mechanical fields [55–57]. Interestingly, the frequency dependence of the electrically poled samples measured parallel and perpendicular to the poling direction are opposite above ~ 150 °C, namely the relative permittivity increases above the as-annealed sample in the parallel case and decreases below the as-annealed samples in the perpendicular case. In previous studies, such a dielectric response was attributed to an anisotropic crystal structure [58]. A corresponding behavior was also found for the mechanically textured samples, whereby the response in parallel and perpendicular direction is inverted. X-ray diffraction data collected parallel and perpendicular to the applied field/stress direction showed variation in field induced domain texture (Figs. SII and SIII) [54], which accounts for the observed directional-dependent behavior. It is important to note, however, that the effect of residual stress on the dielectric properties for the electrically and mechanically loaded samples remains unclear and requires additional investigation. With further increasing temperature above ~ 300 °C, however, the dielectric response was found to be independent of the poling history, indicating that any remanent changes to the material through electrical or mechanical fields were eliminated.

The similarities of the temperature-dependent permittivity of NBT and nonergodic relaxors, like NBT-BT in the vicinity of the MPB [27,48], might be due to one of the following three reasons. Firstly, it is possible that the samples were not fully electrically poled or mechanically textured as a consequence of the large coercive field [59] and coercive stress observed in NBT. However, the piezoelectric coefficient d_{33} of the poled sample was characterized with a custom experimental arrangement, described in detail elsewhere [48,49], revealing a value of 76 pC/N at room temperature for a

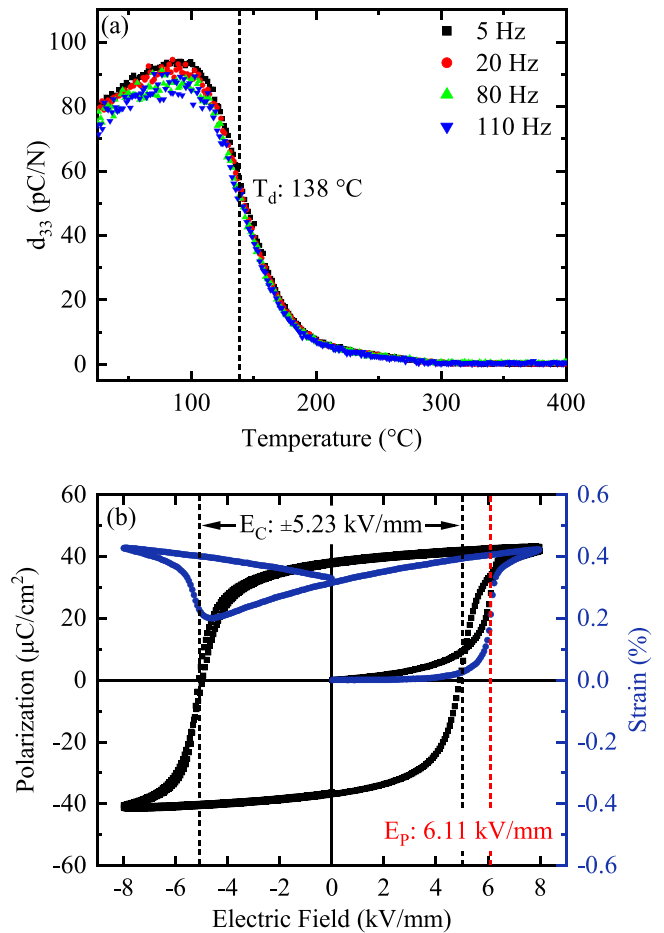


FIG. 2. (a) Temperature-dependent d_{33} of electrically poled NBT and (b) P-E/S-E loops for NBT with poling field E_p and coercive field E_c measured at 100 mHz. In the case of the P-E response both the behavior of an as-annealed and of an electrically poled sample are depicted.

measurement frequency of 110 Hz [Fig. 2(a)], which is in good agreement with literature values [60]. In the case of the mechanically textured samples, the coercive stress was also exceeded, as it can be seen in Fig. 8. Secondly, NBT can potentially exhibit a mixed state at room temperature that consists of both normal ferroelectric and relaxor, as previously suggested for La-doped $(\text{Bi}_{0.5}\text{Na}_{0.41}\text{K}_{0.09})\text{TiO}_3$ [61]. In this state, electrical poling would presumably result in ferroelectric domain wall motion in the ferroelectric volume fraction and a metastable long-range order in the relaxor state, where the relative volume fractions of each component would affect the macroscopic constitutive behavior. Thirdly, the relaxor-like behavior might be attributed to the complex structure of NBT related to octahedra tilting/rotation, A-site cation ordering, and displacement [8,39,62]. Rao *et al.* [25,63] reported that these structural features induce strain heterogeneities, interrupting the long-range order. Similarly, Dorcet *et al.* [14] show the presence of tetragonal platelets in the rhombohedral matrix, which are closely related to the structural heterogeneities. It has been suggested that these platelets enable a cationic displacement in more random directions in the region

between the platelets and the matrix, again giving rise to a relaxor-like behavior.

The directional-dependent relative permittivity further highlights differences between NBT and nonergodic relaxors. Schader *et al.* [41] showed the uniaxial compressive stress- and electric field-dependent dielectric permittivity as a function of temperature for NBT-6BT, which is understood to be a nonergodic relaxor at room temperature. Importantly, both mechanical and electrical fields demonstrated analogous behavior, marked by the formation of a dielectric anomaly and decrease in relative permittivity below T_{F-R} . In contrast, the measurements presented here on NBT reveal a direction dependence relative to the applied field direction, where dielectric measurement directions perpendicular to one another for the electrically and mechanically samples show analogous behavior. This is expected for ferroelectric and ferroelastic domain wall motion, where the induced domain orientations relative to the applied field are not the same for both cases; an electric field should align domains parallel to the measurement direction and a uniaxial compressive stress should induce ferroelectric domains perpendicular to the stress axis. This difference in observed behavior between NBT and NBT-BT can be attributed to the different underlying mechanisms. In nonergodic relaxors, such as NBT-BT, the decisive factor is the ferroelectric long-range order induced through external fields, which shows no directional dependence, whereas the response of NBT is determined by the directional-dependent domain switching process. In this case the varying alignment of the elongated unit cell by electrical poling and mechanical texturing has to be taken into consideration. The application of an electrical field aligns the elongated unit cell in the direction of the field, whereas a mechanical load aligns by means of non-180° domain switching in a plane perpendicular to it [64] (see also Sec. III E). Therefore, a comparability is achieved if the electrically poled sample measured in parallel direction is compared with the mechanically textured sample measured in the perpendicular direction and vice versa. Otherwise the mechanically induced reduction in extrinsic contributions to the dielectric response through, for example, the development of an internal residual stress or the decrease in domain wall density is possible [65–67].

Figure 2(a) shows the temperature-dependent direct piezoelectric coefficient of electrically poled NBT. The d_{33} exhibits a maximum of 85 pC/N (110 Hz) at $\sim 92^\circ\text{C}$ and subsequently decays over a broad temperature range up to 200°C (d_{33} : ~ 7 pC/N), vanishing around 300°C , which is 23°C below T_m . Above this temperature, a frequency dependence of the piezoelectric response is no longer present. Interestingly, the range of decaying d_{33} ($\sim 110^\circ\text{C}$) observed here is significantly larger than that of polycrystalline ferroelectrics, such as soft doped PZT [49], as well as of nonergodic relaxor, e.g., NBT-6BT, which showed a sharp decrease over a narrow temperature range on the order of few $^\circ\text{C}$ followed by a gradual decay over $\sim 50^\circ\text{C}$ [48,68]. The depolarization temperature T_d , taken as the inflection point in the decrease of d_{33} , was found to be 138°C . Previously reported values of T_d range from 161°C to 210°C , depending on the measurement technique used [42]. Investigations of the stress-dependent piezoelectric response demonstrated that external stress was able to increase the depolarization temperature range of both

ferroelectrics [49] and relaxors [69], indicating that residual stresses introduced by, e.g., strain heterogeneity [25,62] or tetragonal platelets in the rhombohedral matrix could have a similar effect [14].

Figure 2(b) displays the room temperature macroscopic bipolar polarization- and strain-electric field hysteresis behavior of as-annealed NBT measured at 100 mHz. During initial application of an electric field, there is a rapid increase in both the polarization (P) and strain (S) at the poling field E_p of 6.11 kV/mm, whereas the coercive field E_C was observed to be 5.23 kV/mm. These results are in good agreement with the previous investigations that have reported E_C values between 5 and 7.3 kV/mm [22,43,68,70]. The wide distribution of E_C might be attributed to either variations in the composition due to the known Bi-volatility [4] that has shown to significantly change the macroscopic electromechanical behavior [71] or variations in measurement frequencies. Interestingly, E_p is $\sim 14\%$ larger than E_C . It is understood that nonergodic relaxors are metastably converted into a long-range ferroelectric order by a sufficiently high electric field, which makes the distinction to normal ferroelectrics difficult [40]. Thereby, the formation of the ferroelectric long-range order requires a different electric field compared to the switching of the pre-existing ferroelectric domains resulting in the deviation of E_p and E_C [27]. It should be mentioned here that also an internal bias field can induce an asymmetric ferroelectric hysteresis and a variation in the critical switching fields [72]. However, our measurement of initially poled NBT did not show any significant difference between the $+E_C$ and the $-E_C$, i.e., the P-E/S-E loop appears symmetric. Therefore, the variation in poling field and the coercive field in NBT is not related to an internal bias field. Hence, the deviation of E_p and E_C might be due to the reduced coherence length of localized octahedral tiling through the initial application of an electric field, reported earlier [25,63].

B. Rate-dependent macroscopic stress-strain response

In order to better elucidate the influence of the relaxor-like behavior in NBT, we have characterized the macroscopic mechanical properties of NBT as a function of loading frequency from 0.01 to 500 mHz for a maximum uniaxial compressive stress of -500 MPa. Previous investigations on relaxor NBT-BT have demonstrated a significant difference in the critical stress for electrically poled and as-annealed samples [27,41,57], making such mechanical measurements a useful tool for investigating the influence of metastable states on the mechanical properties, such as an electric-field induced long-range ferroelectric order [27,41,57]. In addition, the mechanical response is a decisive factor for the application of NBT in capacitors, piezoelectric, and electrochemical devices [27,28]. High internal or external stresses may arise, e.g., due to the strain incompatibility of neighboring grains or due to thermal expansion mismatch of different components and can, therefore, lead to changes in electromechanical properties or failure [27,28].

The room temperature mechanical constitutive behavior of as-annealed and electrically poled NBT at different representative measurement frequencies is shown in Figs. 3(a)–3(d) and 3(e)–3(h), respectively. During initial loading, all stress-

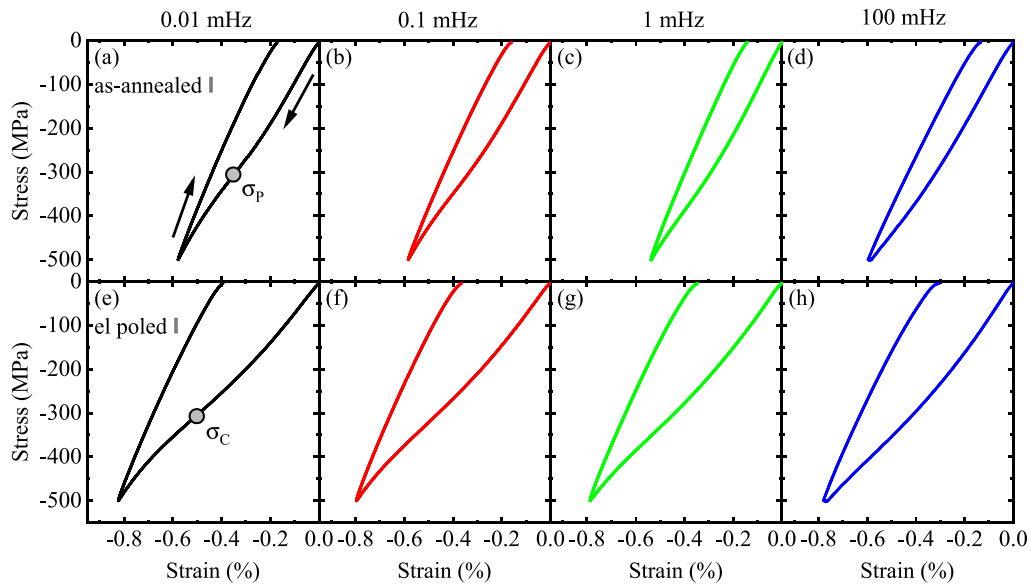


FIG. 3. Stress-strain-curves of as-annealed (a)–(d) and electrically poled (e)–(h) NBT at different frequencies. σ_p and σ_c mark the poling and coercive stress, respectively. Arrows indicate the loading direction.

strain curves show a linear mechanical response, defined by the elastic modulus. With an increasing mechanical load, the stress-strain behavior displays an apparent nonlinearity due to hysteretic processes. In ferroelastic materials this is understood to be caused by the nucleation and growth of ferroelastic domains [64,73], whereas previous works on relaxors have demonstrated that the formation of a long-range ferroelectric order can result in a ferroelastic-like stress-strain response [74]. The critical stress required to induce these remanent effects is defined as the inflection point in the stress-strain curves during loading denoted as poling stress (σ_p) and coercive stress (σ_c) for the as-annealed and poled samples, respectively. As previously noted, E_p and E_c differ by $\sim 14\%$ at a frequency of 100 mHz, while the difference between σ_p and σ_c is $\sim 8\%$ for the same loading frequency. For NBT-7BT, the higher σ_p was attributed to higher mechanical energy required to induce the long-range order compared to normal ferroelastic domain switching [12]. It is important to note that previous investigations on normal ferroelectric/ferroelastic materials revealed that the critical stress did not show a significant variation with poling condition [47,63,75] in contrast to recent reports on relaxor materials that demonstrate a similar behavior to that observed here [27,30,76]. This suggests that NBT, at least from the macroscopic measurements, does not behave entirely like a ferroelectric. Following mechanical unloading, there is the development of a remanent strain, where electrical poling results in a significant increase in remanent strain. Such behavior is expected as a sample poled in the direction of the applied uniaxial compressive stress exhibits an increased number of non- 180° domains preferentially aligned for ferroelastic reorientation, which has been observed for both ferroelectrics and nonergodic relaxors [27,64].

Figure 4 summarizes the characteristic values of σ_p , σ_c , and the remanent strain for all measured frequencies from 0.01 to 500 mHz. The error bars shown, were determined by calculating the error range of five measurements on the same sample at a frequency of 5 mHz and subsequently applied

to the other frequencies. Here it was assumed that a minor misalignment of the samples is the primary reason for the estimated error. The poling stress increases with frequency from $-306 \text{ MPa} \pm 9 \text{ MPa}$ (0.01 mHz) to values exceeding the measurement range of -500 MPa at a frequency of 500 mHz,

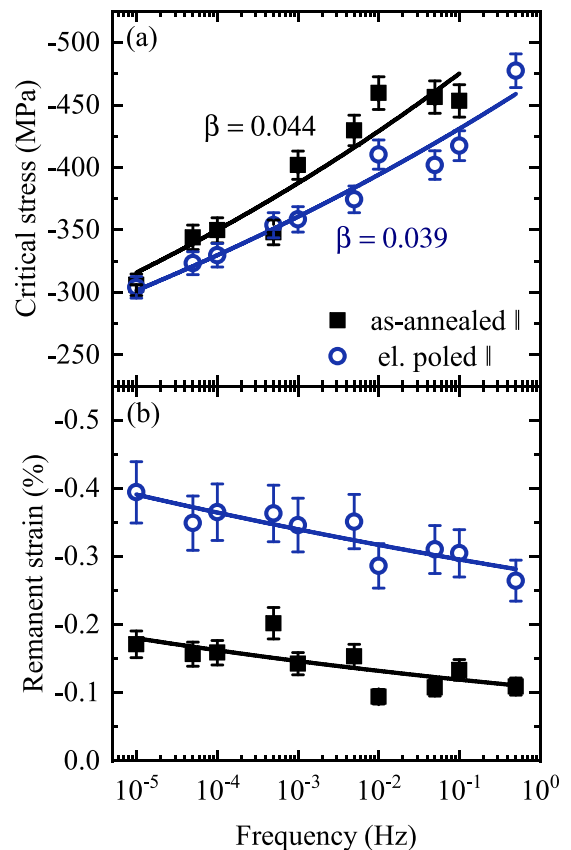


FIG. 4. Frequency-dependent poling stress σ_p , coercive stress σ_c (a) and remanent strain (b) of as-annealed and electrically poled NBT at room temperature.

whereas the coercive stress increases from a comparable value of $-304 \text{ MPa} \pm 9 \text{ MPa}$ to only $-477 \text{ MPa} \pm 14 \text{ MPa}$. On the other hand, the remanent strain decreased from $-0.17\% \pm 0.02\%$ to $-0.11\% \pm 0.01\%$ and $-0.39\% \pm 0.04\%$ to $-0.26\% \pm 0.03\%$ for as-annealed and poled samples, respectively. This gives rise to a comparable change of 36% for the as-annealed and 33% for the poled condition.

Both ferroelectrics and relaxors show a significant frequency-dependent mechanical response. Numerous investigations have shown this for the ferroelectric behavior [75–78]. However, frequency-dependent mechanical properties are scarcely available [27,79,80]. The primary difference between ferroelectrics and relaxors is that the underlying mechanism responsible for the frequency-dependent behavior changes due to the poling process in nonergodic relaxor, whereas domain wall nucleation and growth is the primary mechanism before and after poling in ferroelectrics. Thus, nonergodic relaxors show a significant deviation of E_P/σ_P and E_C/σ_C with measurement frequency due to the different kinetics of each mechanism [27]. In the as-annealed state, the material response of a nonergodic relaxor is determined by the formation of a field-induced ferroelectric long-range order from the previously present PNRs. Whereas in the poled state, the ferroelectric order was previously established by the electrical poling procedure, and the dominant process is domain switching. In the case of normal ferroelectrics, a difference in E_P/σ_P and E_C/σ_C is usually considered to be due to an internal bias field [81].

On the basis of the Kolmogorov-Avrami-Ishibashi (KAI) model [82,83] the frequency dependence of E_C can be approximated. In this model, a power-law relationship between E_C and the frequency f is established, such that $E_C \propto f^\beta$. The exponent β represents the effective dimension of the switching domains and the wave form of the applied field. This was adapted for the poling and coercive stress, where β was determined to be 0.044 and 0.039, respectively. Similar values can be obtained for the remanent strain due to a decreasing saturation of the switching process with increasing frequency and a correlated reduction of the remanent strain, as shown in Figs. 3 and 4(b). Interestingly, the values of the as-annealed samples are in good agreement with polycrystalline rhombohedral PZT in the electrical case (β : 0.04542–0.04863) [77], which might be attributed to the same

crystal structure and therefore, a comparable domain switching process. The well-known relaxor NBT-7BT exhibits in the same frequency range (mechanical measurements) β values of 0.053 and 0.032 for the as-annealed and poled state [27], respectively. It is apparent that the variance in β values is higher compared to the current study. This suggests that the influence of the stress-induced long-range ferroelectric order on the mechanical properties of NBT is not as pronounced as previously shown for NBT-7BT, corresponding well to the observed temperature-dependent dielectric behavior. As such it further indicates that the response of NBT is not similar to the nonergodic nature of NBT-BT. Importantly, however, it should be noted that the β values are smaller than the KAI model would usually assume. However, the same observations were made in earlier reports and attributed to the predomination of domain nucleation and growth mechanisms in the observed low frequency range [27,77].

C. Domain structure (TEM)

The domain structure of NBT was analyzed by TEM. Figures 5(a) and 5(c) show the complex morphology. Within the grains differently sized and shaped domains are observed. An additional fine domain structure is visible inside of large lamellar-like domains (few hundred nanometers) [Fig. 5(b)]. According to SAED analysis, faint superstructure reflections in the $[110]_{pc}$ direction are present [see SAED pattern in Fig. 5(c)].

The present results correspond well with previous investigations [14,37–39]. The domains were described as a fine twin-domain structure (10 to 50 nm) embedded in larger regular domains with a size of several hundred nanometers [39] or as a mixture of fine lamellar, needle-shaped domains (in combination with tetragonal platelets [14]) next to curved undefined domains [38]. However, relaxors generally show diffuse nanosized patterns, where respective PNRs have a size of few nanometers [84,85]. Furthermore, the superlattice reflection, as summarized by Yao *et al.* [62], can have three origins: oxygen octahedral tilting/rotation, chemical ordering of the A site, as well as antiparallel displacement of cations. It is important to note that the analysis performed for this article did not reveal an obvious ordering of the Na and Bi cations. Recently it has been suggested that the octahedral

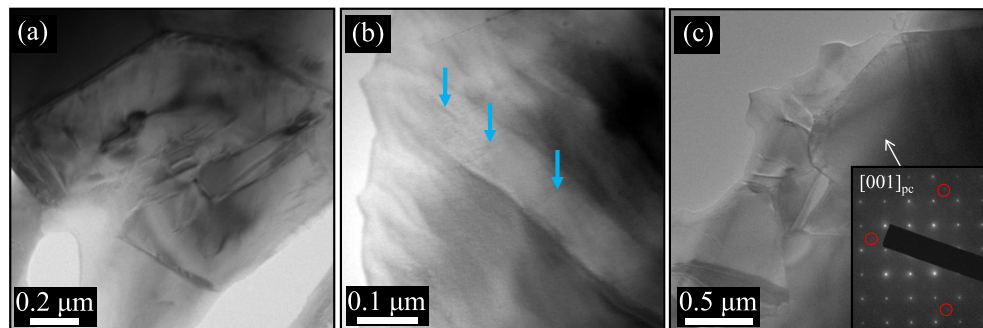


FIG. 5. TEM images at different magnification showing (a) NBT grain with complex domain structure, (b) lamellar-like, few hundred nanometers large domain with embedded fine domain structure (marked by blue arrows), (c) NBT grain with corresponding SAED pattern in $[001]_{pc}$ zone axis index in pseudocubic notation (pc). Red circles mark superlattice reflections in the $[110]_{pc}$ direction.

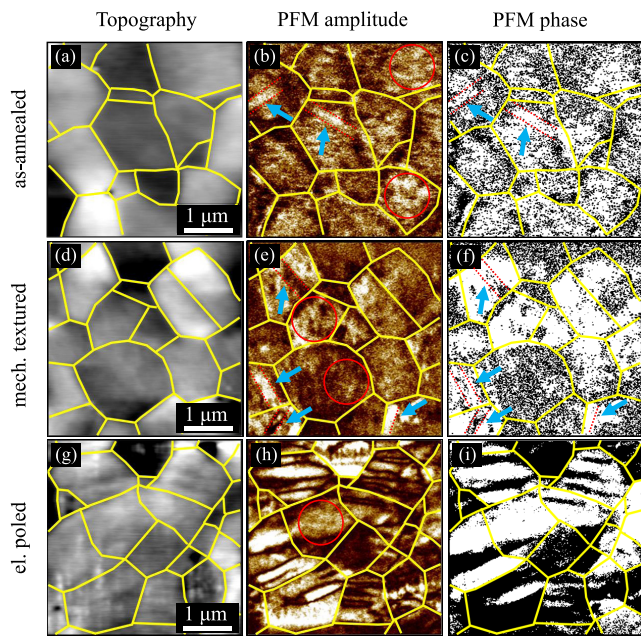


FIG. 6. Representative topography, PFM amplitude and phase image of NBT in the as-annealed state, mechanically textured and electrically poled. Examples of regular and irregular shaped domains are marked by blue arrows plus red dotted lines and red circles, respectively.

rotation and hence the superlattice reflections may originate from tetragonal platelets embedded in a rhombohedral matrix. This is expected to increase the degree of freedom for cationic displacement in between the areas of platelets and matrix and thus be responsible for the relaxor-like behavior [14]. A similar approach is based on the assumption that the described structural features induce strain heterogeneities to interrupt the long-range order [25,63]. Nevertheless, the observed domain structure in the as-annealed NBT indicates that the composition cannot be considered as nonergodic relaxor-like NBT-BT.

D. Stress- and electric field-dependent domain structure

In order to investigate the effect of external electrical and mechanical fields on the local domain structure, PFM was performed on as-annealed, mechanically textured, and electrically poled NBT samples (Fig. 6). Prior to characterization for mechanical texturing and electrical poling compressive stress of -750 MPa at room temperature and an electrical field of 4 kV/mm at 80°C , followed by field cooling, were applied, respectively. Both values are well above their respective critical values, suggesting that remanent changes in the local domain structure are possible. All studied samples have similar grain size around $1\ \mu\text{m}$. The as-annealed and mechanically textured samples displayed similar results, namely, large regular ferroelectric domains of a few hundred nanometers are observed in agreement with TEM analysis. Representative examples of these domains are marked by blue arrows and dotted red lines in Fig. 6. In addition to these large regular structures, a few tens of nanometer large domains are also observed (marked by red circles). These domains appear more irregular

in shape. On the other hand, in the electrically poled sample, the ferroelectric domains are larger, exceeding the size of a few hundred nanometers. This is expected, because during the poling procedure the small domains merge into larger areas due to the rotation of the polarization in the direction of the electric field [86]. Some smaller domains are also observed in this electrically poled sample (marked by red circle in the PFM amplitude image).

In contrast, Martin *et al.* [57] showed the formation of larger domains by both electrical and mechanical fields for the nonergodic relaxor NBT-7BT, which again demonstrates the difference to NBT. The deviation in domain structure of the mechanical and electrical cases might be attributed to the difference in the domain switching process. By application of mechanical stress only non- 180° domain switching is possible. Hence the elongated unit cells are aligned perpendicular to the applied mechanical field direction (see also Sec. III E), whereas electrical poling aligns the domains parallel to the applied field direction. Moreover, the results indicate that ferroelectric and ferroelastic domains in NBT are not related, which was assumed in previous publications [87]. In summary, the PFM investigations of the as-annealed, mechanically textured, and electrically poled samples highlight the complex domain morphology of NBT. The origin of relaxor-like response is possibly related to this complexity. As such the coalescence of nanometer sized domains as well as the switching of the macroscopic domains with electric field and/or mechanical stress induces a relaxor-like electromechanical response.

E. In situ Stress-dependent crystal structure

To gain further insight to the relaxor-like nature of NBT and to better understand the transient mechanisms during mechanical loading, *in situ* synchrotron x-ray diffraction was performed. Figure 7(a) shows the diffraction patterns collected for the sample at the preload load of -25 MPa, maximum load (~ -750 MPa), and after unloading to preload, revealing the change in crystal structure perpendicular to the applied loading direction. A total of 161 diffraction images were recorded during the loading-unloading cycle; representative stress steps are depicted in Fig. 7(b). With increasing stress, the 111_{pc} peak intensity increases at the expense of the $11\bar{1}_{\text{pc}}$ peak intensity. The associated shift of the 200_{pc} reflection to lower 2θ angles indicates the expansion of the d-spacings perpendicular to the applied loading direction, which is almost recovered during unloading [see also Fig. 8(c)]. In contrast, the relative change in $111_{\text{pc}}/11\bar{1}_{\text{pc}}$ peak intensity remains approximately the same during unloading.

Figure 8(a) shows the macroscopic stress-strain curve generated with the same loading-unloading profile of the *in situ* measurement, whereby the poling stress exhibits a value of -330 MPa and a minor back-switching during unloading can be seen. In comparison, Fig. 8(b) summarized the stress-dependent intensity change of the $111_{\text{pc}}/11\bar{1}_{\text{pc}}$ peak calculated at each stress step. The inflection point and hence the maximum rate of the change in intensity is determined to be -371 MPa. After reaching maximum load the intensity ratio remains constant, while removing the load. However, the 200_{pc} lattice strain (combination of intrinsic lattice strain

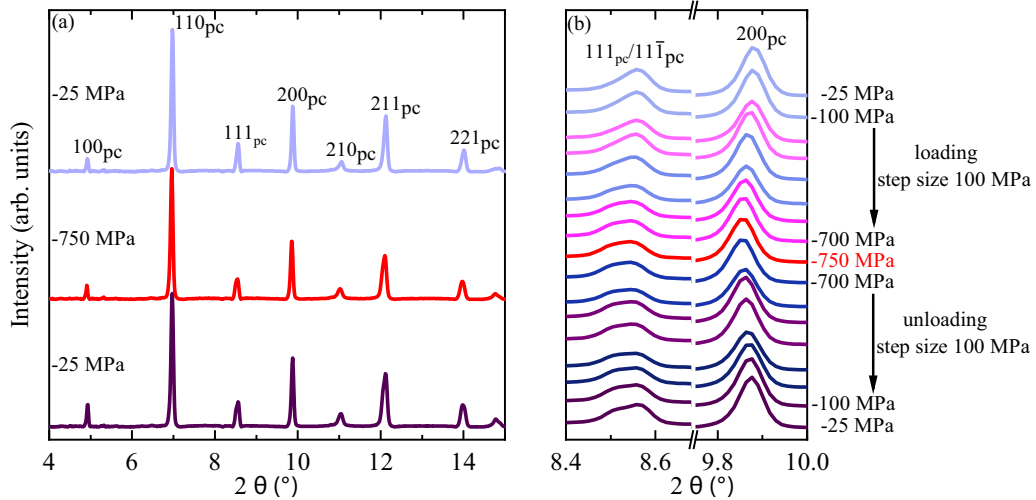


FIG. 7. Room temperature synchrotron x-ray diffraction patterns of NBT (a) as well as evolution of the $111_{pc}/11\bar{1}_{pc}$ and 200_{pc} reflections as a function of stress perpendicular to the applied uniaxial load (b).

and the extrinsic domain switching strain), as illustrated in Fig. 8(c), exhibits almost no discontinuities during the loading-unloading cycle, resulting in a lattice strain of approximately -0.05% .

During loading, ferroelastic domain reorientation begins once the critical stress is reached, resulting in an initially linear slope of the strain-strain diagram [Fig. 8(a)] as well as in the minor change in intensity [Figs. 7(b) and 8(b)]. Above a certain threshold stress, the domain switching rate increases and reaches a maximum, which is defined as the poling stress [88]. The calculated poling stress of the macroscopic measurement is ~ 40 MPa lower than the inflection point estimated from the *in situ* diffraction data. A possible reason might be a minor deviation in the loading rate or slight misalignment of the sample. Nevertheless, the values agree with the previous results of the rate-dependent measurements (see Sec. III B). Further increase in stress up to the maximum load results in a saturation of the switching process and hence in a linear elastic macroscopic mechanical response and a reduced change in intensity. During unloading, the intensity ratio does not

change significantly. This indicates a minor back-switching of domains by means of intergranular coupling stress and domain pinning [89,90]. Thus, there is only a small deviation from the linear elastic behavior during unloading in the stress-strain diagram comparable to soft PZT [91]. If the path of the 200_{pc} lattice strain during the loading-unloading cycle and the remanent strain is considered, it can be assumed that the 200_{pc} strain is constrained by the intergranular stresses, which, despite the high applied mechanical load, have not been reduced by, e.g., microcracking [92,93]. These results reveal a stress-induced lattice strain and domain switching without any apparent phase transformation. Moreover, the structural analysis highlights that the average crystallographic symmetry of NBT is not significantly influenced by the uniaxial compressive stress as high as -750 MPa. It has to be noted that previous reports demonstrated a field-induced transition from the monoclinic to the rhombohedral structure in NBT [94,95]. However, detailed studies have shown that the observed structural change was most likely due to a reduction in strain heterogeneities and coherence length of localized

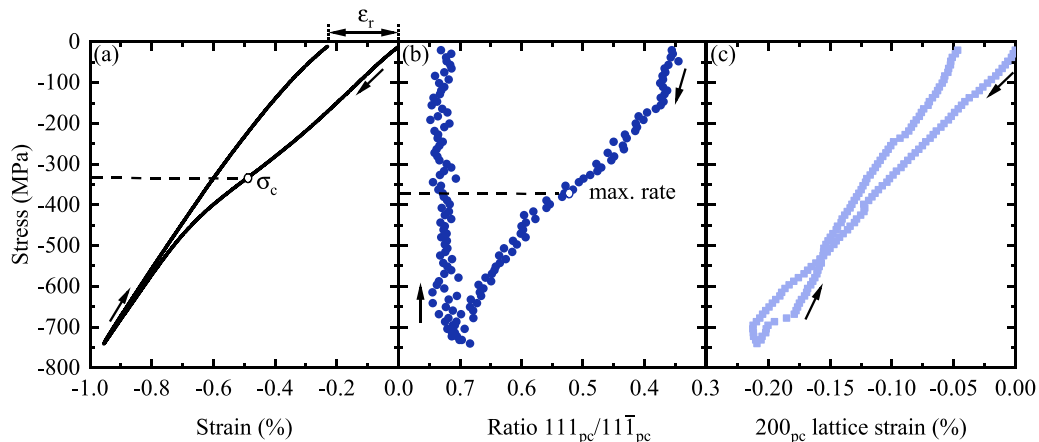


FIG. 8. Comparison of macroscopic stress-strain measurement (a), stress-dependent *in situ* change of the $111_{pc}/11\bar{1}_{pc}$ intensity ratio (b) and 200_{pc} lattice strain (c), respectively. σ_c and the maximum rate are marked. Arrows indicate the loading direction.

octahedra tiling, making the rhombohedral structure visible on a global length [25,63]. Nevertheless, the *in situ* x-ray data, in conjunction with TEM and PFM analysis, indicates that the relaxor-like nature of NBT is due to the field-induced changes in domain structures without any crystallographic phase transition.

Our analysis highlights the origin of the relaxor-like nature of stoichiometric NBT bulk ceramics. The measurements of macroscopic mechanical properties, such as temperature-dependent permittivity of the unpoled, electrically poled, and mechanically textured ceramics clearly reveals that the NBT is neither a classical ferroelectric nor a conventional relaxor. From the analysis of domain structures as well as the crystal structure, it seems the NBT contains signatures of both the relaxors and ferroelectrics. However, the extent of dominating relaxor or ferroelectric nature is possibly highly influenced by the ceramic processing condition, e.g., sintering condition and proper control of Bi-stoichiometry. The peculiar relaxor-like response of NBT originates from their complex crystal and domain structure.

IV. CONCLUSION

The mechanical properties of NBT were characterized over a wide frequency range to gain insight into the relaxor-like behavior, whereby a small deviation in the frequency dependence of the poling stress and coercive stress were obtained. Occurring variations in the crystal and domain structure due to the application of an external uniaxial stress were examined *in*

situ and *ex situ*, respectively. It was concluded that during mechanical loading domains are ferroelastically switched and no structural phase transformation occurs. A change in domain structure by means of PFM analyzes could not be determined. Together with the TEM results, which reveal a complex domain morphology, the material exhibits ferroelectric/-elastic characteristics rather than relaxor properties. Interestingly, electrical poling results in an apparent change of the domain structure, represented by an increased domain size. Additionally, the frequency dependence of the relative permittivity at room temperature is reduced to the same extent by electrical poling and mechanical texturing (excluding mechanically textured in the perpendicular direction), but no clear T_{F-R} is formed. If these results are compared with the characteristic features of relaxors defined by Cross, NBT cannot be defined as a classical relaxor. In fact, these properties are most likely determined by the complex crystal and domain structure.

ACKNOWLEDGMENTS

K.R., N.H.K., A.M., and K.G.W. gratefully acknowledge the support from the Deutsche Forschungsgemeinschaft under WE4972/2 and GRK2495/H as well as the DAAD under Project No. 57402168 as part of the PPP Slovenian Program. H.U. and A.B gratefully acknowledge the support from the Slovenian Research Agency (bilateral project BI-DE-20/21-012, programme P2-0105 and project J2-2497). H.U. thanks to J. Cilensek and T. Klavzar for assistance in the laboratory, B. Kmet is acknowledged for TEM sample preparation.

-
- [1] J. Rödel, W. Jo, K. T. P. Seifert, E. M. Anton, T. Granzow, and D. Damjanovic, *J. Am. Ceram. Soc.* **92**, 1153 (2009).
- [2] A. Chauhan, S. Patel, and R. Vaish, *AIP Adv.* **4**, 087106 (2014).
- [3] M. Li, M. J. Pietrowski, R. A. De Souza, H. Zhang, I. M. Reaney, S. N. Cook, J. A. Kilner, and D. C. Sinclair, *Nat. Mater.* **13**, 31 (2014).
- [4] T. Frömling *et al.*, *J. Mater. Chem. C* **6**, 738 (2018).
- [5] G. A. Smolenskii, V. A. Isupov, A. I. Agranovskaya, and N. N. Krainik, *Sov. Phys. Solid State* **2**, 2982 (1960).
- [6] J. A. Zvirgzds, P. P. Kapostin, J. V. Zvirgzde, and T. V. Kruzina, *Ferroelectrics* **40**, 75 (1982).
- [7] S. B. Vakhrušev, V. A. Isupov, B. E. Kvyatkovsky, N. M. Okuneva, I. P. Pronin, G. A. Smolensky, and P. P. Syrnikov, *Ferroelectrics* **63**, 153 (1985).
- [8] G. Jones and P. Thomas, *Acta Crystallogr. Sect. B* **58**, 168 (2002).
- [9] S. Gorfman and P. A. Thomas, *J. Appl. Crystallogr.* **43**, 1409 (2010).
- [10] E. Aksel, J. S. Forrester, J. L. Jones, P. A. Thomas, K. Page, and M. R. Suchomel, *Appl. Phys. Lett.* **98**, 152901 (2011).
- [11] E. Aksel, J. S. Forrester, J. C. Nino, K. Page, D. P. Shoemaker, and J. L. Jones, *Phys. Rev. B* **87**, 104113 (2013).
- [12] B. N. Rao, A. N. Fitch, and R. Ranjan, *Phys. Rev. B* **87**, 060102(R) (2013).
- [13] V. Dorcet, G. Trolliard, and P. Boullay, *J. Magn. Magn. Mater.* **321**, 1758 (2009).
- [14] V. Dorcet and G. Trolliard, *Acta Mater.* **56**, 1753 (2008).
- [15] R. Beanland and P. A. Thomas, *Scr. Mater.* **65**, 440 (2011).
- [16] K. Sakata and Y. Masuda, *Ferroelectrics* **7**, 347 (1974).
- [17] L. E. Cross, *Ferroelectrics* **151**, 305 (1994).
- [18] R. Sommer, N. K. Yushin, and J. J. van der Klink, *Phys. Rev. B* **48**, 13230 (1993).
- [19] J. Suchanicz, *J. Mater. Sci.* **37**, 489 (2002).
- [20] S.-E. Park, S.-J. Chung, and I.-T. Kim, *J. Am. Ceram. Soc.* **79**, 1290 (1996).
- [21] W. Jo, S. Schaab, E. Sapper, L. A. Schmitt, H. J. Kleebe, A. J. Bell, and J. Rödel, *J. Appl. Phys.* **110**, 074106 (2011).
- [22] M. K. Niranjana, T. Karthik, S. Asthana, J. Pan, and U. V. Waghmare, *J. Appl. Phys.* **113**, 194106 (2013).
- [23] D. K. Khatua, T. Mehrotra, A. Mishra, B. Majumdar, A. Senyshyn, and R. Ranjan, *Acta Mater.* **134**, 177 (2017).
- [24] A. Mishra, D. K. Khatua, A. De, B. Majumdar, T. Fromling, and R. Ranjan, *Acta Mater.* **164**, 761 (2019).
- [25] B. N. Rao, R. Datta, S. S. Chandrashekarana, D. K. Mishra, V. Sathe, A. Senyshyn, and R. Ranjan, *Phys. Rev. B* **88**, 224103 (2013).
- [26] J. Kreisel, P. Bouvier, B. Dkhil, P. A. Thomas, A. M. Glazer, T. R. Welberry, B. Chaabane, and M. Mezouar, *Phys. Rev. B* **68**, 014113 (2003).
- [27] A. Martin, N. H. Khansur, K. Riess, and K. G. Webber, *J. Eur. Ceram. Soc.* **39**, 1031 (2019).
- [28] A. Fossdal, M. Menon, I. Wærnhus, K. Wiik, M.-A. Einarsrud, and T. Grande, *J. Am. Ceram. Soc.* **87**, 1952 (2004).
- [29] M. S. Senousy, R. K. N. D. Rajapakse, D. Mumford, and M. S. Gadala, *Smart Mater. Struct.* **18**, 045008 (2009).
- [30] A. Martin, N. H. Khansur, and K. G. Webber, *J. Eur. Ceram. Soc.* **38**, 4623 (2018).
- [31] L. E. Cross, *Ferroelectrics* **76**, 241 (1987).

- [32] V. V. Shvartsman and D. C. Lupascu, *J. Am. Ceram. Soc.* **95**, 1 (2012).
- [33] J. Suchanicz, *Mater. Sci. Eng. B* **55**, 114 (1998).
- [34] V. A. Isupov, *Ferroelectrics* **315**, 123 (2005).
- [35] J. Suchanicz, I. P. Mercurio, P. Marchet, and T. V. Kruzina, *Phys. Status Solidi B* **225**, 459 (2001).
- [36] I. G. Siny, C. S. Tu, and V. H. Schmidt, *Phys. Rev. B* **51**, 5659 (1995).
- [37] J. Yao, L. Yan, W. Ge, L. Luo, J. Li, D. Viehland, Q. Zhang, and H. Luo, *Phys. Rev. B* **83**, 054107 (2011).
- [38] M. Otonicar, S. D. Skapin, and B. Jancar, *IEEE Trans. Ultrason. Ferroelectr. Freq. Control* **58**, 1928 (2011).
- [39] I. Levin and I. M. Reaney, *Adv. Funct. Mater.* **22**, 3445 (2012).
- [40] A. Bokov and Z. G. Ye, *J. Mater. Sci.* **41**, 31 (2006).
- [41] F. H. Schader, Z. Wang, M. Hinterstein, J. E. Daniels, and K. G. Webber, *Phys. Rev. B* **93**, 134111 (2016).
- [42] E. Aksel, J. S. Forrester, B. Kowalski, M. Deluca, D. Damjanovic, and J. L. Jones, *Phys. Rev. B* **85**, 024121 (2012).
- [43] E. Aksel, J. S. Forrester, H. M. Foronda, R. Dittmer, D. Damjanovic, and J. L. Jones, *J. Appl. Phys.* **112**, 054111 (2012).
- [44] J. Suchanicz and J. Kwapulinski, *Ferroelectrics* **165**, 249 (1995).
- [45] J. Kreisel, A. M. Glazer, P. Bouvier, and G. Lucazeau, *Phys. Rev. B* **63**, 174106 (2001).
- [46] M. Matsuura, H. Iida, K. Hirota, K. Ohwada, Y. Noguchi, and M. Miyayama, *Phys. Rev. B* **87**, 064109 (2013).
- [47] K. G. Webber, E. Aulbach, T. Key, M. Marsilius, T. Granzow, and J. Rödel, *Acta Mater.* **57**, 4614 (2009).
- [48] F. H. Schader, M. Morozov, E. T. Wefring, T. Grande, and K. G. Webber, *J. Appl. Phys.* **117**, 194101 (2015).
- [49] F. H. Schader, D. Isaia, M. Weber, E. Aulbach, and K. G. Webber, *J. Mater. Sci.* **53**, 3296 (2018).
- [50] K. Thangavelu, R. Ramadurai, and S. Asthana, *AIP Adv.* **4**, 017111 (2014).
- [51] J. Suchanicz, *Ferroelectrics* **172**, 455 (1995).
- [52] A. Molak and J. Suchanicz, *Ferroelectrics* **189**, 53 (1996).
- [53] V. Bobnar, Z. Kutnjak, R. Pirc, and A. Levstik, *Phys. Rev. B* **60**, 6420 (1999).
- [54] See Supplemental Material at <http://link.aps.org/supplemental/10.1103/PhysRevB.103.094113> for temperature-dependent dielectric loss and *ex situ* x-ray diffraction data of the electrically poled and mechanically textured $\text{Na}_{1/2}\text{Bi}_{1/2}\text{TiO}_3$.
- [55] C. Randall, D. Barber, R. Whatmore, and P. Groves, *Ferroelectrics* **76**, 277 (1987).
- [56] X. Tan, C. Ma, J. Frederick, S. Beckman, and K. G. Webber, *J. Am. Ceram. Soc.* **94**, 4091 (2011).
- [57] A. Martin, H. Uršič, T. Rojac, and K. G. Webber, *Appl. Phys. Lett.* **114**, 052901 (2019).
- [58] Y. Hiruma, H. Nagata, and T. Takenaka, *J. Appl. Phys.* **105**, 084112 (2009).
- [59] M. Chen, Q. Xu, B. H. Kim, B. K. Ahn, J. H. Ko, W. J. Kang, and O. J. Nam, *J. Eur. Ceram. Soc.* **28**, 843 (2008).
- [60] B. Jaffe, W. R. Cook, and H. Jaffe, *Piezoelectric Ceramics* (Academic, London, 1971), Vol. 1.
- [61] T. H. Dinh *et al.*, *J. Eur. Ceram. Soc.* **36**, 3401 (2016).
- [62] J. Yao, W. Ge, Y. Yang, L. Luo, J. Li, D. Viehland, S. Bhattacharyya, Q. Zhang, and H. Luo, *J. Appl. Phys.* **108**, 064114 (2010).
- [63] B. N. Rao, L. Olivi, V. Sathe, and R. Ranjan, *Phys. Rev. B* **93**, 024106 (2016).
- [64] D. Zhou, M. Kamlah, and D. Munz, *J. Am. Ceram. Soc.* **88**, 867 (2005).
- [65] G. Arlt, D. Hennings, and G. d. With, *J. Appl. Phys.* **58**, 1619 (1985).
- [66] P. Zheng, J. L. Zhang, Y. Q. Tan, and C. L. Wang, *Acta Mater.* **60**, 5022 (2012).
- [67] Y. Huan, X. Wang, J. Fang, and L. Li, *J. Am. Ceram. Soc.* **96**, 3369 (2013).
- [68] W. Jo, R. Dittmer, M. Acosta, J. Zang, C. Groh, E. Sapper, K. Wang, and J. Rödel, *J. Electroceram.* **29**, 71 (2012).
- [69] F. H. Schader, G. A. Rossetti, J. Luo, and K. G. Webber, *Acta Mater.* **126**, 174 (2017).
- [70] T. Takenaka, K. O. Sakata, and K. O. Toda, *Ferroelectrics* **106**, 375 (1990).
- [71] J. Carter, E. Aksel, T. Iamsasri, J. S. Forrester, J. Chen, and J. L. Jones, *Appl. Phys. Lett.* **104** (2014).
- [72] L. Jin, F. Li, and S. Zhang, *J. Am. Ceram. Soc.* **97**, 1 (2014).
- [73] W. J. Merz, *Phys. Rev.* **95**, 690 (1954).
- [74] K. G. Webber, M. Vögler, N. H. Khansur, B. Kaeswurm, J. E. Daniels, and F. H. Schader, *Smart Mater. Struct.* **26**, 063001 (2017).
- [75] Z. Chen, Y. Zhang, S. Li, X.-M. Lu, and W. Cao, *Appl. Phys. Lett.* **110**, 202904 (2017).
- [76] S. M. Yang *et al.*, *Phys. Rev. B* **82**, 174125 (2010).
- [77] X. Chen, X. Dong, H. Zhang, F. Cao, G. Wang, Y. Gu, H. He, and Y. Liu, *J. Am. Ceram. Soc.* **94**, 4165 (2011).
- [78] S. Hashimoto, H. Orihara, and Y. Ishibashi, *J. Phys. Soc. Jpn.* **63**, 1601 (1994).
- [79] D. Zhou, R. Wang, and M. Kamlah, *J. Eur. Ceram. Soc.* **30**, 2603 (2010).
- [80] A. Menzel, A. Arockiarajan, and S. M. Sivakumar, *Smart Mater. Struct.* **17**, 015026 (2008).
- [81] A. B. Kounga, T. Granzow, E. Aulbach, M. Hinterstein, and J. Rödel, *J. Appl. Phys.* **104**, 024116 (2008).
- [82] Y. Ishibashi and Y. Takagi, *J. Phys. Soc. Jpn.* **31**, 506 (1971).
- [83] Y. Ishibashi and H. Orihara, *Integr. Ferroelectr.* **9**, 57 (1995).
- [84] U. Prah *et al.*, *J. Mater. Chem. C* **8**, 3452 (2020).
- [85] M. Yoshida, S. Mori, N. Yamamoto, Y. Uesu, and J. M. Kiat, *Ferroelectrics* **217**, 327 (1998).
- [86] M. Kratzer, M. Lasnik, S. Röhrig, C. Teichert, and M. Deluca, *Sci. Rep.* **8**, 422 (2018).
- [87] J. Yao, W. Ge, L. Luo, J. Li, D. Viehland, and H. Luo, *Appl. Phys. Lett.* **96**, 222905 (2010).
- [88] J. Forrester and E. Kisi, *J. Eur. Ceram. Soc.* **24**, 595 (2004).
- [89] A. Pramanick, D. Damjanovic, J. E. Daniels, J. C. Nino, and J. L. Jones, *J. Am. Ceram. Soc.* **94**, 293 (2011).
- [90] D. Zhou and M. Kamlah, *Acta Mater.* **54**, 1389 (2006).
- [91] M. I. Morozov, M.-A. Einarsrud, J. R. Tolchard, P. T. Geiger, K. G. Webber, D. Damjanovic, and T. Grande, *J. Appl. Phys.* **118**, 164104 (2015).
- [92] N. H. Khansur, T. Rojac, D. Damjanovic, C. Reinhard, K. G. Webber, J. A. Kimpton, and J. E. Daniels, *J. Am. Ceram. Soc.* **98**, 3884 (2015).
- [93] J.-T. Reszat, A. E. Glazounov, and M. J. Hoffmann, *J. Eur. Ceram. Soc.* **21**, 1349 (2001).
- [94] B. N. Rao and R. Ranjan, *Phys. Rev. B* **86**, 134103 (2012).
- [95] T.-M. Usher, I. Levin, J. E. Daniels, and J. L. Jones, *Sci. Rep.* **5**, 14678 (2015).